PHILOSOPHICAL TRANSACTIONS A

royalsocietypublishing.org/journal/rsta

Research

Cite this article: Cartes C, Tirapegui E, Pandit R, Brachet M. 2022 The Galerkin-truncated Burgers equation: crossover from inviscid-thermalized to Kardar–Parisi–Zhang scaling. *Phil. Trans. R. Soc. A* **380**: 20210090. https://doi.org/10.1098/rsta.2021.0090

Received: 12 May 2021
Accepted: 22 July 2021

One contribution of 14 to a theme issue 'Scaling the turbulence edifice (part 2)'.

Subject Areas:
fluid mechanics, statistical physics

Keywords:
truncated Burgers equation, Kardar–Parisi–Zhang universality, crossover

Author for correspondence:
M. Brachet
e-mail: marc-etienne.brachet@ens.fr

The Galerkin-truncated Burgers equation: crossover from inviscid-thermalized to Kardar–Parisi–Zhang scaling

C. Cartes[1], E. Tirapegui[2], R. Pandit[3] and M. Brachet[4]

[1]Complex Systems Group, Facultad de Ingeniería y Ciencias Aplicadas, Universidad de los Andes, Santiago, Chile
[2]Departamento de Física, Universidad de Chile, Santiago, Chile
[3]Department of Physics, Centre for Condensed Matter Theory, Indian Institute of Science, Bangalore 560012, India
[4]Laboratoire de Physique de l'École Normale Supérieure, ENS, Université PSL, CNRS, Sorbonne Université, Université de Paris, Paris 75005, France

ET, 0000-0001-9402-625X; MB, 0000-0002-0618-5806

The one-dimensional Galerkin-truncated Burgers equation, with both dissipation and noise terms included, is studied using spectral methods. When the truncation-scale Reynolds number $R_{\min}$ is varied, from very small values to order 1 values, the scale-dependent correlation time $\tau(k)$ is shown to follow the expected crossover from the short-distance $\tau(k) \sim k^{-2}$ Edwards–Wilkinson scaling to the universal long-distance Kardar–Parisi–Zhang scaling $\tau(k) \sim k^{-3/2}$. In the inviscid limit, $R_{\min} \to \infty$, we show that the system displays *another* crossover to the Galerkin-truncated inviscid-Burgers regime that admits thermalized solutions with $\tau(k) \sim k^{-1}$. The scaling forms of the time-correlation functions are shown to follow the known analytical laws and the skewness and excess kurtosis of the interface increments distributions are characterized.

This article is part of the theme issue 'Scaling the turbulence edifice (part 2)'.

1. Introduction

Galerkin-truncated hydrodynamical systems, which retain only a finite number of Fourier modes, have been studied actively in fluid mechanics [1–5].

THE ROYAL SOCIETY PUBLISHING

In his pioneering work [1] of 1952, T.D. Lee showed that these truncated systems satisfy Liouville's theorem and that, assuming ergodicity, there is energy equipartition among the spectral modes. Later, Kraichnan [4] proposed a different approach for these *absolute equilibrium* states by considering that the complex amplitudes of the Fourier modes followed a canonical distribution that is controlled by the mean values of the invariants of the system. The Galerkin-truncated hydrodynamical system that has been investigated most extensively is the time-reversible Euler equation for a classical, ideal fluid [6–8], which can be studied efficiently, in a spatially periodic domain, by the Fourier pseudospectral method [9,10]. Absolute-equilibrium solutions have also been examined in a variety of hydrodynamical systems including compressible flows [11], the Gross-Pitaevskii equation in both three and two dimensions [12,13], and the Euler equation and ideal magnetohydrodynamics (MHD) in two dimensions [14].

These results on thermalization in hydrodynamical systems are well known in the fluid-dynamics community, but less known than they deserve to be in the area of non-equilibrium statistical mechanics. To bridge this gap between these related fields, we carry out a systematic study of the relaxation to absolute equilibrium in the one-dimensional inviscid Burgers equation, perhaps the simplest hydrodynamical system demonstrating absolute equilibration. The initial stages of the thermalization are known to involve the formation of oscillatory structures, which have been named *tygers* [15–17]. The typical relaxation time near the absolute equilibrium can be studied conveniently via the scale-dependent correlation time $\tau(k)$, which can be computed from the time-dependent correlation function. It is known to scale as $\tau(k) \sim k^{-1}$ [18–20]. Note that the same k^{-1}-scaling law is known to take place in the truncated three-dimensional Euler equation [6]. Thus $\tau(k)$ cannot be simply related to an eddy turnover time defined from the equilibrium energy spectrum that scales as $E(k) \sim k^{d-1}$ in d-dimensions.

Adding noise and dissipation terms to the one-dimensional inviscid Burgers equation (see equation (4.14) of reference [21]) transforms it into the Kardar–Parisi–Zhang (KPZ) equation [22–25] that is well known in non-equilibrium statistical mechanics. The KPZ equation admits the same exact equilibrium probability distribution as the inviscid Burgers equation.[1] However, the one-dimensional KPZ correlation time around equilibrium is known to have a $k^{-3/2}$ scaling. The different time-correlation scalings k^{-1} and $k^{-3/2}$ around the same equilibrium for the inviscid truncated Burgers equation and the KPZ equation are the main motivation for the present work. Note that there is also a third (trivially linear) viscous type of scaling known as the Edwards-Wilkinson [26] (EW) scaling k^{-2} that arises when the nonlinear term is negligible. In the following, we will characterize the crossover behaviour between these different regimes in terms of the Reynolds number estimated at the truncation scale. Let us stress that the dissipative and inviscid truncated Burgers equation admit the same equilibrium only with the noise correlations considered here. For studies of the one-dimensional Burgers equation with differently correlated noises, see e.g. [27–31]; these studies concentrate on intermittency of equal-time structure functions and not the time correlations we investigate.

The remainder of this paper is organized as follows. Section 2 contains the system's definitions, with special attention given to spectral truncation, conserved quantities and stationary probabilities. Section 3 is devoted to our numerical results: after defining the algorithms and physical parameters, the scalings of the correlation times and the distributions of the interface increments are characterized. Finally, our conclusions are given in §4.

2. System definitions

We consider the randomly forced, generalized one-dimensional Burgers equation that is defined by the following stochastic partial differential equation for the velocity field $u(x,t)$ (e.g. [21–24,32–35]):

$$\partial_t u + \lambda u \partial_x u = \nu \partial_{xx} u + \sqrt{D}\partial_x f, \tag{2.1}$$

[1]In only one dimension. In dimensions greater than 1, the inviscid Burgers equations does not conserve the energy (e.g. [21]).

royalsocietypublishing.org/journal/rsta Phil. Trans. R. Soc. A 380: 20210090

where λ is the coefficient of the nonlinear term, ν is the kinematic viscosity, D a diffusion coefficient and f is a zero-mean, Gaussian force with variance

$$\langle f(x,t)f(x',t')\rangle = 2\pi\delta(x-x')\delta(t-t'). \tag{2.2}$$

If we define $u \equiv \partial_x h$, i.e.

$$h(x,t) = \int_0^x u(y,t)\,\mathrm{d}y \tag{2.3}$$

we obtain the KPZ equation

$$\partial_t h + \frac{\lambda}{2}(\partial_x h)^2 = \nu\partial_{xx}h + \sqrt{D}f. \tag{2.4}$$

We contrast the following three cases in our study: (i) the deterministic, inviscid, one-dimensional Burgers equation, with $\lambda = 1$, $\nu = 0$, and $D = 0$; (ii) the Edwards–Wilkinson (EW) equation, with $\lambda = 0$, $\nu > 0$ and $D > 0$; and (iii) the KPZ equation, with $\lambda > 0$, $\nu > 0$ and $D > 0$.

(a) Spectral truncation and conserved quantities

Henceforth, we consider 2π-periodic boundary conditions in x. We introduce the Fourier representation

$$u(x,t) = \sum_{k=-\infty}^{\infty} \hat{u}(k,t)\exp(ikx), \tag{2.5}$$

where the caret denotes a spatial Fourier transform, $u(x,t) \in \mathbb{R}$, so $\hat{u}(-k,t) = \overline{\hat{u}(k,t)}$; complex conjugation is indicated by the overline. Using

$$\frac{u^2(x,t)}{2} = \frac{1}{2}\sum_{n,p=-\infty}^{\infty} \hat{u}_{n-p}(t)\hat{u}_p(t)\mathrm{e}^{inx}, \tag{2.6}$$

the unforced and inviscid Burgers equation (equation (2.1) with $\nu = 0$, $\lambda = 1$ and $D = 0$) can be written as

$$\partial_t \hat{u}(k,t) = -\frac{ik}{2}\sum_{p=-\infty}^{\infty} \hat{u}_{k-p}(t)\hat{u}_p(t), \tag{2.7}$$

which conserves the total energy

$$\begin{aligned} E &= \frac{1}{2\pi}\int_0^{2\pi} \frac{u(x,t)^2}{2}\,\mathrm{d}x \\ &= \frac{1}{2}\sum_{k=-\infty}^{\infty} |\hat{u}(k,t)|^2. \end{aligned} \tag{2.8}$$

Note that integrating by parts the nonlinear term in (2.1) shows that the integrals $I_n(t) = \int_0^{2\pi} u(x,t)^n dx$ are all conserved by the inviscid dynamics (2.7) (the energy corresponding to the case $n = 2$).

Let us now spectrally truncate (or Galerkin truncate) this system. To do this, we need to *enforce* that, for $k > k_{\max}$, $\hat{u}(k,t) = 0$ and $\partial_t\hat{u}(k,t) = 0$. To wit, we introduce the Galerkin projector $\mathcal{P}$ that reads in Fourier space

$$\mathcal{P}_G[\hat{u}_k] = \theta(k_{\max} - |k|)\hat{u}_k, \tag{2.9}$$

where $\theta(k) = 1$, if $k \le k_{\max}$ and $\theta(k) = 0$, if $k > k_{\max}$. Galerkin truncation amounts to the replacements $u := \mathcal{P}_G[u]$, $u\partial_x u := \mathcal{P}_G[u\partial_x u]$ and $f := \mathcal{P}_G[f]$ in equation (2.1), thus reducing (2.7) to a finite number of ordinary differential equations.

The Galerkin-truncated version of (2.7) thus reads, for $-k_{\max} \le k \le k_{\max}$,

$$\partial_t \hat{u}(k,t) = -\frac{ik}{2} \sum_{\sup(-k_{\max}, k-k_{\max})}^{\inf(k_{\max}, k+k_{\max})} \hat{u}_{k-p}(t)\hat{u}_p(t), \tag{2.10}$$

or, in a more symmetrical form,

$$\partial_t \hat{u}(k,t) = -\frac{ik}{2} \sum_{p,q} \delta_{k,p+q}\theta(k_{\max} - |p|)\theta(k_{\max} - |q|)\hat{u}_p(t)\hat{u}_q(t), \tag{2.11}$$

where δ denotes the Kronecker symbol. Thus, the nonlinear truncated term explicitly reads:

$$\mathcal{N}_k(\hat{u}) = -\frac{ik}{2} \sum_{p,q} \delta_{k,p+q}\theta(k_{\max} - |k|)\theta(k_{\max} - |p|)\theta(k_{\max} - |q|)\hat{u}_p\hat{u}_q. \tag{2.12}$$

It is straightforward to check out that the nonlinear term (2.12) verifies the following relations:

$$\left.\begin{aligned} 0 &= \mathcal{N}_0(\hat{u}), \\ 0 &= \sum_k \hat{u}_{-k}\mathcal{N}_k(\hat{u}), \\ \text{and} \qquad 0 &= \sum_{k,p,q} \delta_{-k,p+q}\theta(k_{\max} - |p|)\theta(k_{\max} - |q|)\hat{u}_p\hat{u}_q\mathcal{N}_k(\hat{u}). \end{aligned}\right\} \tag{2.13}$$

Thus, three conservation laws survive the Galerkin truncation and

$$\left.\begin{aligned} P &= \hat{u}_0, \\ E &= \frac{1}{2}\sum_{k=-k_{\max}}^{k_{\max}} |\hat{u}(k,t)|^2, \\ \text{and} \qquad H &= \sum_{k,p,q} \delta_{-k,p+q}\theta(k_{\max} - |k|)\theta(k_{\max} - |p|)\theta(k_{\max} - |q|)\hat{u}_k\hat{u}_p\hat{u}_q \end{aligned}\right\} \tag{2.14}$$

are *still* conserved after truncation.

The conserved quantities P and E are, respectively, the momentum and the energy of the system. The third surviving conserved quantity H can be used to provide an explicit Hamiltonian formulation of the truncated system. It is known to play a role in the thermalization dynamics only for very special choices of the initial conditions [36].

In our direct numerical simulations, we use a standard Fourier pseudospectral method, with dealiasing performed by the 2/3 rule. Clearly, such a pseudospectral method is identical to a spectral Galerkin method (e.g. [9]). We use N collocation points and spectral truncation is performed for $k > k_{\max} = [N/3]$, where $[\cdot]$ denotes the integer part. Note that with this choice of dealiasing, the third conserved quantity H must be evaluated as $\mathcal{P}_G[u\mathcal{P}_G[u^2]]$. If one instead insists, as done in [18,19,36], to evaluate it simply as $\mathcal{P}_G[u^3]$ then the truncation must be performed for $k \ge k_{\max} = [N/4]$. Both truncated system and conserved quantities are identical (when H is evaluated correctly). Therefore, here we will use the 2/3 scheme that allows us to use more modes for a given resolution.

(b) Stationary probability

The nonlinear truncated term (2.12) verifies the Liouville property

$$\sum_k \frac{\partial \mathcal{N}_k(\hat{u})}{\partial \hat{u}_k} = 0. \tag{2.15}$$

In the case of absolute equilibrium of the deterministic, inviscid, one-dimensional Burgers equation truncated system, a standard argument (e.g. [1,4,5]) is that the microcanonical

royalsocietypublishing.org/journal/rsta Phil. Trans. R. Soc. A 380: 20210090

distribution

$$P_{\mathrm{mc}}[u] = Z_{\mathrm{mc}}^{-1}\delta(E(u) - E), \tag{2.16}$$

when the number of degrees of freedom $2k_{\max}+1$ is large enough, can be well approximated by the canonical distribution

$$P_{\mathrm{sta}}[u] = Z_c^{-1}\mathrm{e}^{-\beta E}, \tag{2.17}$$

where Z_{mc} and Z_c denote normalization factors.

A direct way to proceed is to introduce the Liouville equation for the probability $\mathbb{P}[\{\hat{u}_k, \hat{u}_k^*\}_{0\le k\le k_{\max}}]$,

$$\frac{\partial \mathbb{P}}{\partial t} = \sum_{0\le k\le k_{\max}} \frac{\partial}{\partial \hat{u}_k}[-\mathcal{N}_k(\hat{u})\mathbb{P}] + \text{c.c}, \tag{2.18}$$

where $\hat{u}_k^* = \hat{u}_{-k}$ is considered as an independent variable and c.c denotes complex conjugation.

It follows directly from energy conservation that (2.18) admits (2.17) as a stationary solution.

Note that the stationary distribution (2.17) is a white noise in space for $u(x)$ and thus a Brownian process for $h(x)$.

In both the EW ($\lambda = 0$, $\nu > 0$ and $D > 0$) and the KPZ cases ($\lambda > 0$, $\nu > 0$ and $D > 0$), the probability distribution $\mathbb{P}$ of the stochastic process defined by equations (2.1) and (2.2) and the spectral truncation (2.9) can be shown to obey the following Fokker–Planck equation [37,38]:

$$\frac{\partial \mathbb{P}}{\partial t} = \sum_{0\le k\le k_{\max}} \frac{\partial}{\partial \hat{u}_k}\left[-(\lambda\mathcal{N}_k(\hat{u}) - \nu k^2\hat{u}_k)\mathbb{P} + Dk^2\frac{\partial \mathbb{P}}{\partial \hat{u}_k^*}\right] + \text{c.c.} \tag{2.19}$$

Let us remark that (2.17) is also a stationary solution of (2.19). Indeed, the nonlinear term in the Fokker–Planck equation can be treated exactly like its counterpart in the Liouville equation (2.18); the remaining terms also cancel for the stationary distribution (2.17), because, in equilibrium, we must have $\nu k^2\hat{u}_k - \beta D k^2\hat{u}_k = 0$, whence we get

$$D = \frac{\nu}{\beta}. \tag{2.20}$$

Defining the *r.m.s.* velocity u_{rms} by averaging over the stationary distribution (2.17)

$$\langle E\rangle = \frac{u_{\mathrm{rms}}^2}{2} = \frac{k_{\max}+1}{\beta}, \tag{2.21}$$

(see equations (2.8) and (2.9)) we find that

$$\beta = \frac{2(k_{\max}+1)}{u_{\mathrm{rms}}^2} \tag{2.22}$$

and

$$D = \frac{\nu u_{\mathrm{rms}}^2}{2(k_{\max}+1)}. \tag{2.23}$$

As the equilibrium probability is determined, we now focus on the time-correlation functions

$$\Gamma(k,\tau) = \langle \hat{u}_k^*(t)\hat{u}_k(t+\tau)\rangle_t. \tag{2.24}$$

In the KPZ case, with the Fokker–Planck equation (2.19), it is well known [21,22] that the existence of a fluctuation dissipation theorem ensures that the associated response function has the same characteristic time-scale as the equilibrium time correlation function. The same fluctuation-dissipation relation (with statistical averaging over initial conditions) [39] also applies in the inviscid noiseless case (2.18).

3. Numerical results

(a) Algorithms

We use standard pseudo-spectral Fourier methods. FFTs are performed on N points and the nonlinear term is truncated at $k_{\max} = N/3$. In order to have a robust method that is also precise, when there is no forcing and dissipation, we timestep by using a fourth order Runge–Kutta (RK) method. For weak viscosities, the same RK timestep is used for the deterministic part (nonlinear and dissipation) and the white noise is added independently, as an extra (explicit) step. The timestep has thus to be smaller than a fraction of $1/(\nu k_{\max}^2)$ and $1/(u_{\rm rms} k_{\max})$. For large viscosities, we use instead the implicit method of reference [40]. The noise intensity D is fixed by using equation (2.23). The initial data are set up as a Gaussian white noise in x with given value of $u_{\rm rms} = \sqrt{2E}$. The time average of the correlation function (2.24) is performed over the same time interval for all wavenumbers. The duration of a run is typically of a few of the largest scale correlation time. At this point, statistical convergence is not optimal for the largest scales. However, computations are performed in parallel for a number (typically $N_{\rm rea} = 128$) of independent realizations of the Gaussian initial conditions (2.17) and Gaussian white noise (2.2). The resulting independent time-averaged correlation functions are further averaged over the $N_{\rm rea}$ realizations. In this way, uniform convergence over the spectrum variable k is obtained.

(b) Physical parameters

Because of our choice of working with 2π periodic boundary conditions, the largest scale L in our simulations is always fixed to $L = 2\pi$. The smallest available scale is resolution dependent and related to the largest wavenumber $k_{\max} = [N/3]$ (equivalently to the collocation mesh size $\Delta x = 2\pi/N$). Thus, a given computation is parametrized by $u_{\rm rms}$, $k_{\max}$ and ν. The initial data used to start the time-integrations is always set to a random Gaussian field (see (2.17)) with the same value of $u_{\rm rms}$ used to fix D to its viscosity-dependent value. Therefore, the $\nu = 0$ (and $D = 0$) case amounts to integrating the inviscid truncated Burgers equation starting from absolute equilibrium initial conditions and, when ν in non-zero, it is the full KPZ system (2.2) (with $\lambda = 1$) that is integrated, also starting from the equilibrium distribution. Thus, in this latter case, one expects to recover the KPZ scaling of the correlation-time in the limit of large spatial scales.

However, the speed of this approach will depend on the value of the parameters at small scale. We introduce a scale-dependent Reynolds number

$$R_e(k) = \frac{u_{\rm rms}}{\nu k}. \tag{3.1}$$

The truncation-scale Reynolds number is given by $R_{\min} = R_e(k_{\max})$, thus $R_{\min} = u_{\rm rms}/\nu k_{\max}$, or

$$R_{\min} = \frac{3}{N\nu} u_{\rm rms}. \tag{3.2}$$

On general grounds, one expects to see EW scaling when $R_{\min} \ll 1$ and recover the inviscid truncated Burgers case in the $R_{\min} \to \infty$ limit that corresponds to $\nu = 0$. In what follows, we will determine the time-scale by fixing $u_{\rm rms} = 1$ and varying ν. We will discuss the crossover in terms of the dimensionless parameter $R_{\min}$.

(c) Scalings of correlation times

We first study the behaviour of the correlation function $\Gamma(k, t)$ by making a series of runs at resolution $N = 1024$ ($k_{\max} = 341$), $u_{\rm rms} = 1$ and various viscosities.

Scaling behaviour is particularly apparent when represented in the $(\log(t), \log(k))$ plane. Indeed, in this logarithmic representation, scaling simply corresponds to equal values of the correlation $\Gamma(k, t)$ along straight lines.

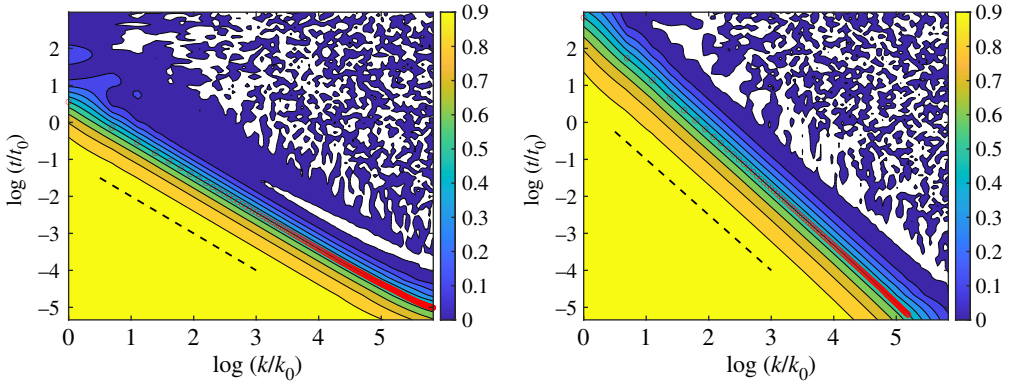

Figure 1. Contour plots of the correlation function $\Gamma(k,t)/\Gamma(k,0)$ represented in the natural logarithm (log(k), log(t)) plane; (*a*) inviscid Burgers scaling obtained at $\nu = 0$; (*b*): KPZ scaling obtained at $\nu = 3.0 \times 10^{-3}$; $\Gamma(k,t)/\Gamma(k,0)$ contour levels are drawn from 0.0 to 0.9 and spaced by 0.1 The dashed black lines indicate (*a*) $t \sim k^{-1}$ and (*b*) $t \sim k^{-3/2}$. The points $t = \tau_{1/2}(k)$, computed independently using $\Gamma(k,\tau_{1/2}) = \frac{1}{2}\Gamma(k,0)$, are indicated by red circles. (Online version in colour.)

Figure 1 shows contour plots of the normalized correlation function $\tilde{\Gamma}(k,t) = \Gamma(k,t)/\Gamma(k,0)$. The red circles[2] indicate the points $t = \tau_{1/2}(k)$. They were computed independently, for each k, by solving the equation $\Gamma(k,\tau_{1/2}) = \frac{1}{2}\Gamma(k,0)$.

Figure 1*a* shows the inviscid Burgers scaling that is obtained for $\nu = 0$, corresponding to an infinite truncation-scale Reynolds number $R_{\min}$. The black dashed line indicates the theoretical $t \sim k^{-1}$ law. On figure 1*b*, the KPZ scaling obtained at $\nu = 3.0 \times 10^{-3}$ is displayed, corresponding to a truncation-scale Reynolds number $R_{\min} = 0.98$. The black dashed lines indicating the theoretical $t \sim k^{-3/2}$ law.

Figure 2*a* demonstrates the EW scaling that is obtained with $\nu = 2.4 \times 10^{-2}$, corresponding to a truncation-scale Reynolds number of $R_{\min} = 0.12$. The viscous $t \sim k^{-2}$ EZ law is indicated by the black dashed line. Figure 2*b* shows the crossover in the scaling of the decorrelation times $\tau_{1/2}(k)$ versus k for various values of the viscosity ν. The crossover behaviour is clearly visible in figure 3 that displays the same data compensated by $k^{3/2}$, so that KPZ scaling corresponds to a horizontal line. The red markers correspond to the EW to KPZ transition with various values of viscosities in geometric progression corresponding to a truncation-scale Reynolds number: $R_{\min} = 0.12$, $R_{\min} = 0.24$, $R_{\min} = 0.48$ and $R_{\min} = 0.98$. The green markers correspond to the KPZ to inviscid transition, with various viscosities, also in geometric progression corresponding to a truncation-scale Reynolds number: $R_{\min} = 1.96$, $R_{\min} = 3.91$, $R_{\min} = 7.71$, $R_{\min} = 15.4$, $R_{\min} = 31.2$, $R_{\min} = 62.3$, $R_{\min} = 124.6$ and $R_{\min} = \infty$. The EW k^{-2} scaling law and the KPZ $k^{-3/2}$ scaling are indicated by solid lines and the inviscid k^{-1} scaling is denoted by a dashed line.

Figure 4 shows the scaling form of the normalized correlation functions $\Gamma(k,t)/\Gamma(k,0)$ versus the rescaled wavenumber, with the same conditions as in figures 1–3.

The left panel shows the KPZ correlation (obtained at $\nu = 0.003$), plotted versus the rescaled variable $k(t/7.0)^{2/3}$ for various values of k. The theoretical correlation function, computed in [41], is shown as a solid black line. The inset provides details on the change of sign of the correlation.

The right panel displays the inviscid ($\nu = 0$) correlation versus the rescaled variable kt, for various values of k. The theoretical short-time parabolic behaviour is shown as a black continuous curve. The inset shows short-times details. The inviscid parabolic law can be obtained by the following arguments. Starting from the equilibrium correlation functions $\langle \hat{u}(k,t)\hat{u}(k',0)\rangle$, we can define the time scale τ_C as the parabolic decorrelation time

$$\tau_C^2 \partial_{tt} \langle \hat{u}(k,t)\hat{u}(k',0)\rangle_{|t=0} = \langle \hat{u}(k,0)\hat{u}(k',0)\rangle, \tag{3.3}$$

[2]Red circles standing right on top of the 0.5 contour line validate the interpolation scheme that we use to draw the contour lines in the logarithmic representation from the equally spaced in time and wavenumber raw data for $\Gamma(k,t)$.

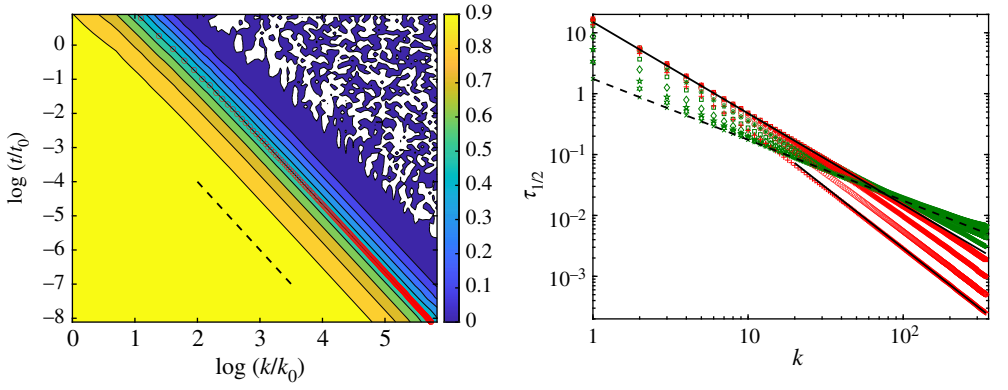

Figure 2. (*a*) Contour plots of the correlation function $\Gamma(k,t)/\Gamma(k,0)$ represented in the natural logarithm ($\log(k)$, $\log(t)$) plane for the EW scaling obtained at $\nu = 2.4 \times 10^{-2}$; contour levels are drawn from 0.0 to 0.9 and spaced by 0.1. The dashed black lines indicate $t \sim k^{-2}$. The points $t = \tau_{1/2}(k)$, computed independently using $\Gamma(k, \tau_{1/2}) = \frac{1}{2}\Gamma(k,0)$, are indicated by red circles. (*b*) Crossover in the scaling of the decorrelation time $\tau_{1/2}$: $\tau_{1/2}$ versus k. Red markers correspond to the EW to KPZ transition: $\nu = 2.4 \times 10^{-2}$: +, $\nu = 1.2 \times 10^{-2}$: o, $\nu = 6.0 \times 10^{-3}$: asterisk and $\nu = 3.0 \times 10^{-3}$: square. Green markers correspond to the KPZ to inviscid transition: $\nu = 1.5 \times 10^{-3}$: +, $\nu = 7.5 \times 10^{-4}$: o, $\nu = 3.8 \times 10^{-4}$: asterisk, $\nu = 1.9 \times 10^{-4}$: square, $\nu = 9.4 \times 10^{-5}$: diamond, $\nu = 4.7 \times 10^{-5}$: pentagram, $\nu = 2.3 \times 10^{-5}$: hexagram, and $\nu = 0$: cross. Scaling laws are indicated by solid lines: EW k^{-2} and KPZ $k^{-3/2}$. The new inviscid k^{-1} scaling is denoted by a dashed line. Runs performed with $k_{\max} = 341$ and $u_{\rm rms} = 1$. (Online version in colour.)

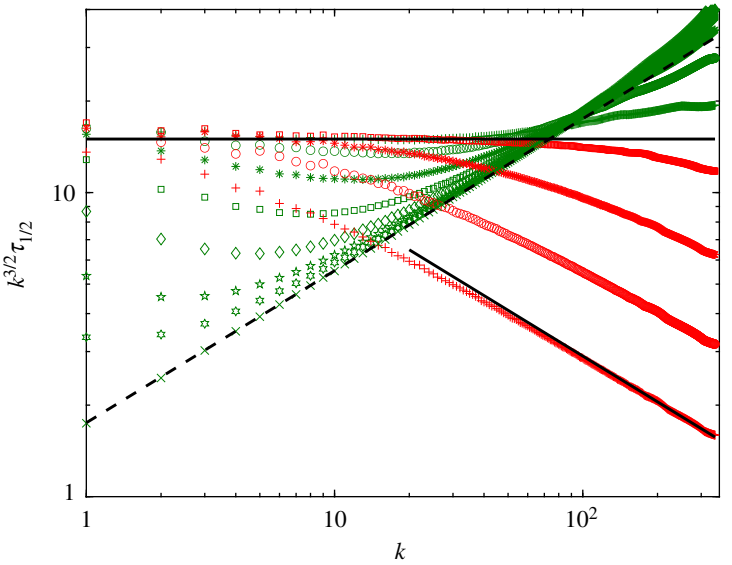

Figure 3. Crossover in the scaling of the decorrelation time $\tau_{1/2}$ for the same conditions as in figure 2*b*, but compensated by $k^{3/2}$: $k^{3/2}\tau_{1/2}$ versus k. Red markers correspond to the EW to KPZ transition: $\nu = 2.4 \times 10^{-2}$: +, $\nu = 1.2 \times 10^{-2}$: o, $\nu = 6.0 \times 10^{-3}$: asterisk and $\nu = 3.0 \times 10^{-3}$: square. Green markers correspond to the KPZ to inviscid transition: $\nu = 1.5 \times 10^{-3}$: +, $\nu = 7.5 \times 10^{-4}$: o, $\nu = 3.8 \times 10^{-4}$: asterisk, $\nu = 1.9 \times 10^{-4}$: square, $\nu = 9.4 \times 10^{-5}$: diamond, $\nu = 4.7 \times 10^{-5}$: pentagram, $\nu = 2.3 \times 10^{-5}$: hexagram, and $\nu = 0$: cross. Scaling laws are indicated by solid lines: EW k^{-2} and KPZ $k^{-3/2}$. The new inviscid k^{-1} scaling is denoted by a dashed line. Runs performed with $k_{\max} = 341$ and $u_{\rm rms} = 1$. (Online version in colour.)

time translation invariance allows us to express the second-order time derivative as

$$-\left\langle \partial_t \hat{u}(k,t)\partial_{t'}\hat{u}(k',t')\right\rangle_{|t=t'=0}. \tag{3.4}$$

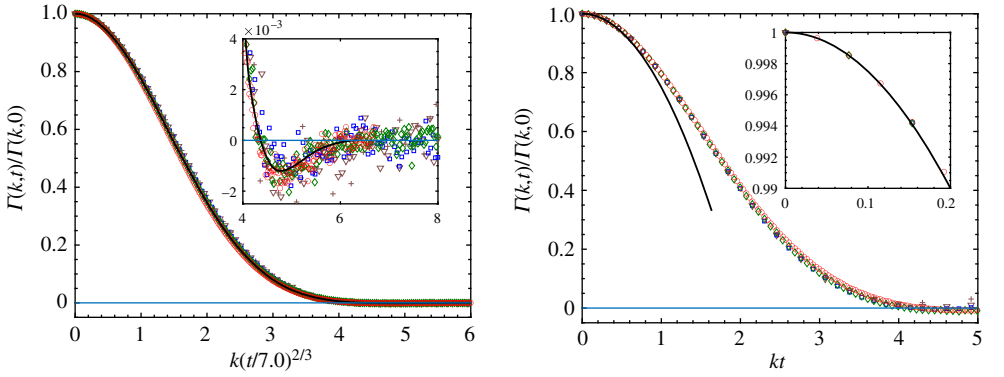

Figure 4. Scaling of correlation functions $\Gamma(k,t)/\Gamma(k,0)$ versus the rescaled wavenumber. (*a*) KPZ ($\nu = 0.003$) correlation versus $k(t/7.0)^{2/3}$ (o: $k = 4$, diamond: $k = 8$, square: $k = 16$, v: $k = 32$ and +: $k = 64$) compared with the theoretical correlation function computed in [41] shown by a solid line (the inset shows the change of sign of the theoretical correlation). (*b*) Inviscid ($\nu = 0$) correlation versus kt (o: $k = 8$, diamond: $k = 16$, square: $k = 32$, v: $k = 64$ and +: $k = 128$) compared with the theoretical short-time parabolic behaviour (see inset and equation (3.5)). Computations were performed with $k_{\max} = 341$ and $u_{\rm rms} = 1$. (Online version in colour.)

Using expressions (2.11) for the time derivatives reduces the evaluation of τ_C to that of an equal-time fourth-order moment of a Gaussian field with correlation $\langle \hat{u}(k,t)\hat{u}(-k,t)\rangle = u_{\rm rms}^2/(2k_{\max}+1)$. The only non-vanishing contribution is a one loop graph [33,42]. The correlation time τ_C associated with wavenumber k is found [6,20] in this way to obey the simple scaling law

$$\tau_C = \frac{\sqrt{2}}{k u_{\rm rms}}, \tag{3.5}$$

and this time scale is proportional to the eddy turnover time [18] at wavenumber k.

It is apparent from the figure that our numerical data obey the theoretical predictions.

(d) Distributions of the interface increments

The seminal work of Prähofer & Spohn [43] was recently referred to as 'the 2nd KPZ Revolution' [24]. It has led to a new set of studies of the one-dimensional KPZ universality class [25,32,44–48]. In particular, [49] notes that, at point x and for large t

$$\delta h = h(x,t) - h(x,0) \approx v_\infty t + (\Gamma t)^{\beta_{\rm KPZ}} \chi_\beta + o(t^{\beta_{\rm KPZ}}), \quad \text{for } t \to \infty, \tag{3.6}$$

where the parameters Γ and v_∞ depend on the model, and $\beta_{\rm KPZ} = 1/3$. Furthermore, χ_β is a random variable distributed according to different (Tracy-Widom) distributions [50] for different initial conditions. For the problem we study, we use Brownian initial data, so we expect (see [49]) to find a Baik-Rains [51] distribution.

Figure 5 shows the evolution of the distributions of the interface increments δh computed with $k_{\max} = 682$ and $u_{\rm rms} = 1$. Figure 5*a* displays the probability distribution functions of δh at various times and $\nu = 3.0 \times 10^{-3}$. The solid black curve indicates the theoretical probability distribution function of [32]. Figure 5*b* shows the time evolution of the skewness S (in green) and excess kurtosis $K - 3$ (in red) at various viscosities.

Figure 6 displays the same data, with a change of sign for the skewness (in order to be comparable with fig. 3 of [49]). Our results indicate a tendency for the viscous run to converge towards the theoretically predicted values, while the inviscid computations only display power law behaviour for the skewness and the excess flatness.

It is apparent on figures 5 and 6 that the theoretically predicted Baik–Rains values for skewness and kurtosis seem to match best the intermediate-viscosity numerical results (square markers:

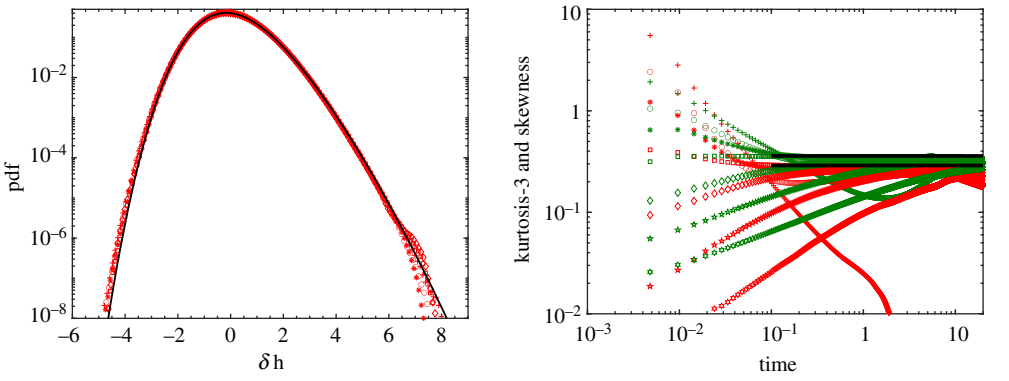

Figure 5. (*a*) Probability distribution functions of the interface increments δh at times $t = 0.5$: +, $t = 1$: o, $t = 2$: asterisk, $t = 4$: square and $t = 8$: diamond, with $\nu = 3.0 \times 10^{-3}$, $k_{max} = 682$ and $u_{rms} = 1$; (*b*) time evolution of the skewness (green) and excess kurtosis (red) at various viscosities in log-log scales. The solid black lines indicate the theoretical results of reference [32]. The markers correspond to: inviscid ($\nu = 0$): +, $\nu = 3.8 \times 10^{-4}$: o, $\nu = 7.5 \times 10^{-4}$: asterisk, $\nu = 1.5 \times 10^{-3}$: square, $\nu = 3.0 \times 10^{-3}$: diamond, $\nu = 6.0 \times 10^{-3}$: pentagram, $\nu = 1.2 \times 10^{-2}$: hexagram. (Online version in colour.)

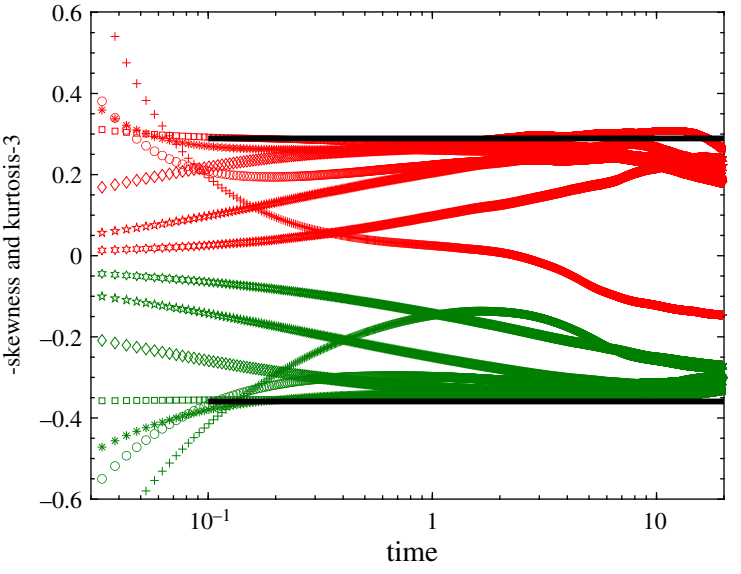

Figure 6. Time evolution of the skewness (green) and excess kurtosis (red) at various viscosities in log-lin scales (same conditions as in figure 5*b*, with a change of sign for the skewness). The solid black lines indicate the theoretical results of [32]. The markers correspond to: inviscid ($\nu = 0$): +, $\nu = 3.8 \times 10^{-4}$: o, $\nu = 7.5 \times 10^{-4}$: asterisk, $\nu = 1.5 \times 10^{-3}$: square, $\nu = 3.0 \times 10^{-3}$: diamond, $\nu = 6.0 \times 10^{-3}$: pentagram, $\nu = 1.2 \times 10^{-2}$: hexagram. (Online version in colour.)

$\nu = 1.5 \times 10^{-3}$). The corresponding truncation-scale Reynolds number (see equation (3.2)) is $R_{min} = 0.98$. As the runs were performed with a fixed ratio of largest to smallest scale (resolution $N = 2048$), it is understandable that, in the limit of very small R_{min}, the results should go to the Gaussian EW limit of zero skewness and excess kurtosis. This simply explains the trends apparent on the figures: short-time skewness and excess kurtosis are too small for small R_{min} and too large for large R_{min}. They however seem to converge, for large times, toward the theoretical values as long as R_{min} remains of order unity. Note that the skewness and kurtosis are known to converge

very slowly with resolution (e.g. [49]) and a precise quantification of these trends therefore needs higher resolution and longer runs and is well beyond the scope of the present paper.

4. Conclusion

By using pseudospectral numerical simulations of the one-dimensional Galerkin-truncated Burgers equation, with noise and dissipation (2.2), we have reproduced the very well known properties of the one-dimensional KPZ universality class such as the $k^{-3/2}$ scaling of the correlation time, the known analytical forms for the rescaled time-correlation function and the rescaled interface increments probability distribution function.

We have characterized a new crossover, controlled by the truncation-scale Reynolds number R_{min}, towards an inviscid regime with correlation time scaling as k^{-1}. This new regime corresponds to the absolute equilibrium solutions of the inviscid noiseless Burgers equation. To obtain this regime, it is crucial that the numerical scheme *exactly* conserves the invariant energy of the system. This inviscid regime should also be present in finite-difference schemes, provided that they also conserve the invariants (see the discussions in [18,19]). On general grounds, one expects that any model within the one-dimensional KPZ universality class could also exhibit this new crossover provided that it also admits *exact conservation laws* in some well-defined non-dissipative limit.

This new regime might be amenable to a renormalization-group analysis, which would have, in addition to the known [22] KPZ stable fixed point and EW unstable fixed point, a new fixed point corresponding to the inviscid regime. This is left for a future work.

Data accessibility. This article has no additional data.

Authors' contributions. All authors participated in the analytical computations. M.B. and R.P. drafted the manuscript. M.B. and C.C. performed the numerical simulations. C.C., R.P. and M.B. read, edited and approved the manuscript. E.T. was instrumental in the early definition of the research project and the corresponding analytical computations. He sadly passed away in 2020 and could not therefore edit and approve the final manuscript.

Competing interests. We declare we have no competing interests.

Funding. This work was supported by the French Agence nationale de la recherche (ANR QUTE-HPC project no. ANR-18-CE46-0013).

Acknowledgements. This work was granted access to HPC resources of MesoPSL financed by Region Ile de France and the project Equip@Meso (reference ANR-10-EQPX-29-01) of the programme Investissements d'Avenir supervised by Agence Nationale pour la Recherche. M.B. and R.P. thank the Indo-French Centre for Applied Mathematics for financial support. R.P. also thanks CSIR, UGC and DST India for support and Dipankar Roy for discussions. C.C., E.T. and M.B. acknowledge the support of the Laboratoire International Associé 'Matière: Structure et Dynamique' LIA-MSD. C.C. wishes to acknowledge the support of FONDECYT (CL), no. 1200357 and Universidad de los Andes (CL) through FAI initiatives. Uriel Frisch has been a leader in research on turbulence for several decades. He has inspired many researchers in this area, especially M.B. and R.P., who have worked closely with him. We wish him many more years of active research and we look forward to working with him.

References

1. Lee TD. 1952 On some statistical properties of hydrodynamical and magneto-hydrodynamical fields. *Q. Appl. Math.* **10**, 69–74. (doi:10.1090/qam/1952-10-01)
2. Hopf E. 1952 Statistical hydromechanics and functional calculus. *J. Ration. Mech. Anal.* **1**, 87–123.
3. Kraichnan R. 1955 On the statistical mechanics of an adiabatically compressible fluid. *J. Acoust. Soc. Am.* **27**, 438–441. (doi:10.1121/1.1907924)
4. Kraichnan R. 1973 Helical turbulence and absolute equilibrium. *J. Fluid Mech.* **59**, 745–752. (doi:10.1017/S0022112073001837)
5. Orszag S. 1977 Statistical theory of turbulence. In *Les Houches 1973: fluid dynamics* (eds R Balian, JL Peube). New York, NY: Gordon and Breach.

6. Cichowlas C, Bonaïti P, Debbasch F, Brachet M. 2005 Effective dissipation and turbulence in spectrally truncated Euler flows. *Phys. Rev. Lett.* **95**, 264502. (doi:10.1103/PhysRevLett.95.264502)
7. Krstulovic G, Mininni PD, Brachet ME, Pouquet A. 2009 Cascades, thermalization, and eddy viscosity in helical Galerkin truncated Euler flows. *Phys. Rev. E* **79**, 1–5. (doi:10.1103/PhysRevE.79.056304)
8. Verma MK. 2020 Boltzmann equation and Hydrodynamic equations: their equilibrium and non-equilibrium behaviour. *Phil. Trans. R. Soc. A* **378**, 20190470. (doi:10.1098/rsta.2019.0470)
9. Gottlieb D, Orszag SA. 1977 *Numerical analysis of spectral methods*. Philadelphia: SIAM.
10. Canuto C, Hussani MY, Quarteroni A, Zang TA. 1988 *Spectral methods in fluid dynamics*. New York, NY and Berlin, Germany: Springer.
11. Krstulovic G, Cartes C, Brachet M, Tirapegui E. 2009 Generation and charecterization of absolute equilibrium of compressible flows. *Int. J. Bifurcation Chaos* **19**, 3445–3459. (doi:10.1142/S021812740902489X)
12. Krstulovic G, Brachet ME. 2011 Dispersive bottleneck delaying thermalization of turbulent Bose-Einstein condensates. *Phys. Rev. Lett.* **106**, 115303. (doi:10.1103/PhysRevLett.106.115303)
13. Shukla V, Brachet M, Pandit R. 2013 Turbulence in the two-dimensional Fourier-truncated Gross-Pitaevskii equation. *New J. Phys.* **15**, 113025. (doi:10.1088/1367-2630/15/11/113025)
14. Krstulovic G, Brachet M-E, Pouquet A. 2011 Alfvén waves and ideal two-dimensional Galerkin truncated magnetohydrodynamics. *Phys. Rev. E* **84**, 016410. (doi:10.1103/PhysRevE.84.016410)
15. Ray SS, Frisch U, Nazarenko S, Matsumoto T. 2011 Resonance phenomenon for the Galerkin-truncated Burgers and Euler equations. *Phys. Rev. E* **84**, 016301. (doi:10.1103/PhysRevE.84.016301)
16. Banerjee D, Ray SS. 2014 Transition from dissipative to conservative dynamics in equations of hydrodynamics. *Phys. Rev. E* **90**, 041001. (doi:10.1103/PhysRevE.90.041001)
17. Ray SS. 2015 Thermalized solutions, statistical mechanics and turbulence: an overview of some recent results. *Pramana* **84**, 395–407. (doi:10.1007/s12043-014-0928-x)
18. Majda AJ, Timofeyev I. 2000 Remarkable statistical behavior for truncated Burgers-Hopf dynamics. *Proc. Natl Acad. Sci. USA* **97**, 12 413–12 417. (doi:10.1073/pnas.230433997)
19. Majda A, Timofeyev I. 2002 Statistical mechanics for truncations of the Burgers-Hopf equation: a model for intrinsic stochastic behavior with scaling. *Milan J. Math.* **70**, 39–96. (doi:10.1007/s00032-002-0003-9)
20. Cichowlas C. 2005 Truncated Euler equation: from complex singularities dynamics to turbulent relaxation. Ph.D. thesis, Universite Pierre et Marie Curie—Paris VI, https://tel.archives-ouvertes.fr/tel-00070819/document.
21. Forster D, Nelson DR, Stephen MJ. 1977 Large-distance and long-time properties of a randomly stirred fluid. *Phys. Rev. A* **16**, 732–749. (doi:10.1103/PhysRevA.16.732)
22. Kardar M, Parisi G, Zhang Y-C. 1986 Dynamic scaling of growing interfaces. *Phys. Rev. Lett.* **56**, 889–892. (doi:10.1103/PhysRevLett.56.889)
23. Halpin-Healy T, Zhang Y-C. 1995 Kinetic roughening phenomena, stochastic growth, directed polymers and all that. Aspects of multidisciplinary statistical mechanics. *Phys. Rep.* **254**, 215–414. (doi:10.1016/0370-1573(94)00087-J)
24. Halpin-Healy T, Takeuchi KA. 2015 A KPZ cocktail-shaken, not stirred.... *J. Stat. Phys.* **160**, 794–814. (doi:10.1007/s10955-015-1282-1)
25. Quastel J, Spohn H. 2015 The one-dimensional KPZ equation and its universality class. *J. Stat. Phys.* **160**, 965–984. (doi:10.1007/s10955-015-1250-9)
26. Edwards SF, Wilkinson DR. 1982 The surface statistics of a granular aggregate. *Proc. R. Soc. Lond. A* **381**, 17–31. (doi:10.1098/rspa.1982.0056)
27. Chekhlov A, Yakhot V. 1995 Kolmogorov turbulence in a random-force-driven Burgers equation: anomalous scaling and probability density functions. *Phys. Rev. E* **52**, 5681–5684. (doi:10.1103/PhysRevE.52.5681)
28. Hayot F, Jayaprakash C. 1996 Multifractality in the stochastic Burgers equation. *Phys. Rev. E* **54**, 4681–4684. (doi:10.1103/PhysRevE.54.4681)
29. Boldyrev SA. 1997 Velocity-difference probability density functions for Burgers turbulence. *Phys. Rev. E* **55**, 6907–6910. (doi:10.1103/PhysRevE.55.6907)

30. Verma MK. 2000 Intermittency exponents and energy spectrum of the Burgers and KPZ equations with correlated noise. *Physica A* **277**, 359–388. (doi:10.1016/S0378-4371(99)00544-0)
31. Mitra D, Bec J, Pandit R, Frisch U. 2005 Is multiscaling an artifact in the stochastically forced Burgers equation? *Phys. Rev. Lett.* **94**, 194501. (doi:10.1103/PhysRevLett.94.194501)
32. Halpin-Healy T, Lin Y. 2014 Universal aspects of curved, flat, and stationary-state Kardar-Parisi-Zhang statistics. *Phys. Rev. E* **89**, 010103. (doi:10.1103/PhysRevE.89.010103)
33. Frisch U. 1995 *Turbulence: the legacy of A. N. Kolmogorov*. Cambridge, UK: Cambridge University Press.
34. Frisch U, Bec J. 2001 Burgulence. In *New trends in turbulence turbulence* (eds M Lesieur, A Yaglom, F. David), pp. 341–383. Berlin, Heidelberg: Springer.
35. Bec J, Khanin K. 2007 Burgers turbulence. *Phys. Rep.* **447**, 1–66. (doi:10.1016/j.physrep.2007.04.002)
36. Abramov RV, Kovačič G, Majda AJ. 2003 Hamiltonian structure and statistically relevant conserved quantities for the truncated Burgers-Hopf equation. *Commun. Pure Appl. Math.* **56**, 1–46. (doi:10.1002/(ISSN)1097-0312)
37. van Kampen NG. 1981 *Stochastic processes in physics and chemistry*. Amsterdam, The Netherlands: Elsevier North-Holland.
38. Langouche F, Roekaerts D, Tirapegui E. 1982 *Functional integration and semiclassical expansions*. Dordrecht, The Netherlands: D Reidel Publishing Compagny.
39. Kraichnan R. 1959 Classical fluctuation-relaxation theorem. *Phys. Rev.* **113**, 1181–1182. (doi:10.1103/PhysRev.113.1181)
40. Mannella V, Palleschi R. 1989 Fast and precise algorithm for computer simulation of stochastic differential equations. *Phys. Rev. A* **40**, 3381–3386. (doi:10.1103/PhysRevA.40.3381)
41. Prähofer M, Spohn H. 2004 Exact scaling functions for one-dimensional stationary KPZ growth. *J. Stat. Phys.* **115**, 255–279. (doi:10.1023/B:JOSS.0000019810.21828.fc)
42. Isserlis L. 1918 On a formula for the product-moment coefficient in any number of variables. *Biometrika* **12**, 134–139. (doi:10.1093/biomet/12.1-2.134)
43. Prähofer M, Spohn H. 2000 Universal distributions for growth processes in $1 + 1$ dimensions and random matrices. *Phys. Rev. Lett.* **84**, 4882–4885. (doi:10.1103/PhysRevLett.84.4882)
44. Sasamoto T, Spohn H. 2010 One-dimensional Kardar-Parisi-Zhang equation: an exact solution and its universality. *Phys. Rev. Lett.* **104**, 230602. (doi:10.1103/PhysRevLett.104.230602)
45. Calabrese P, Le Doussal P. 2011 Exact solution for the Kardar-Parisi-Zhang equation with flat initial conditions. *Phys. Rev. Lett.* **106**, 250603. (doi:10.1103/PhysRevLett.106.250603)
46. Imamura T, Sasamoto T. 2012 Exact solution for the stationary Kardar-Parisi-Zhang equation. *Phys. Rev. Lett.* **108**, 190603. (doi:10.1103/PhysRevLett.108.190603)
47. Corwin I. 2012 The Kardar-Parisi-Zhang equation and universality class. *Random Matrices: Theory Appl.* **1**, 1130001. (doi:10.1142/S2010326311300014)
48. Saberi AA, Dashti-Naserabadi H, Krug J. 2019 Competing universalities in Kardar-Parisi-Zhang growth models. *Phys. Rev. Lett.* **122**, 040605. (doi:10.1103/PhysRevLett.122.040605)
49. Roy D, Pandit R. 2020 One-dimensional Kardar-Parisi-Zhang and Kuramoto-Sivashinsky universality class: limit distributions. *Phys. Rev. E* **101**, 030103. (doi:10.1103/PhysRevE.101.030103)
50. Tracy CA, Widom H. 1994 Level-spacing distributions and the Airy kernel. *Commun. Math. Phys.* **159**, 151–174. (doi:10.1007/BF02100489)
51. Baik J, Rains EM. 2000 Limiting distributions for a polynuclear growth model with external sources. *J. Stat. Phys.* **100**, 523–541. (doi:10.1023/A:1018615306992)